Materials Science Forum
ISSN: 1662-9752, Vol. 1186, pp 47-57
doi:10.4028/p-92DAUf
© 2026 The Author(s). Published by Trans Tech Publications Ltd, Switzerland.
Submitted: 2026-01-19
Revised: 2026-02-13
Accepted: 2026-02-26
Online: 2026-04-16

ML-Based Prediction of Tool Kinematics in Cold Forging of Tailored Hollow Shafts with Variable Wall Thickness

Alexander Weiß[1,a*] and Mathias Liewald[1,b]

[1]University of Stuttgart, Institute for Metal Forming Technology (IFU), Holzgartenstraße 17, 70174 Stuttgart, Germany

[a*]alexander.weiss@ifu.uni-stuttgart.de, [b]mathias.liewald@ifu.uni-stuttgart.de

[*]corresponding author

Keywords: cold forging, variable wall thickness, tool kinematic prediction.

Abstract. The production of tailored hollow shafts usually requires multiple manufacturing processes such as multi-stage forming processes and subsequently several machining operations, resulting into high costs and high manufacturing times. To address these challenges, a novel cold forging process featuring an adjustable forming zone was developed by the authors. This new approach enables the production of tailored hollow shafts with varying cross-sections in their length direction as well as internal undercuts within one stroke of the ram.In order to achieve the desired target geometry of a hollow shaft, a specific tool kinematic is required to precisely adjust the cross-section of the forming zone during the process. Currently, determining geometry-specific tool kinematics requires a time consuming iterative numerical procedure. In this paper, a machine learning approach for the prediction of the tool kinematics for a given target geometry of a tailored hollow shaft with variable wall thickness in its length direction is presented.

Introduction

In view of strict EU climate targets, the reduction of CO_2 emissions has become a central challenge for industry, especially in the manufacturing sector [1]. Consequently, improvements in resource efficiency remain a fundamental objective, particularly in high-volume manufacturing processes such as cold forging. Hollow shafts are widely used in several technical fields and play an important role within lightweight design strategies. They offer a significant weight-saving potential compared to solid shafts while maintaining high structural performance [2]. This concept is further advanced by the implementation of tailored hollow shafts with variable wall thicknesses. Such load-adapted components allow for the distribution of material strictly according to the specific load requirements, e.g., within a drive system.

However, the manufacturing of such tailored hollow shafts is currently associated with considerable effort and high costs. Conventional production routes often require complex process chains, combining multiple forming stages with subsequent machining operations to achieve the final workpiece geometry [3]. These extensive process chains not only lead to high cycle times and manufacturing costs but are also limited in terms of geometric flexibility, as certain features cannot be realised with all standard forming methods.

To address these limitations, a novel cold forging process featuring an adjustable forming zone was developed by the authors [4, 5]. The process is based on a conventional hollow forward extrusion process, with the difference that the mandrel is connected to a separate hydraulic cylinder, allowing it to be moved independently of the hollow punch and the die. The mandrel has at least two different cross-sections which can be positioned within the forming zone of the die. This leads to different cross-sections of the forming zone and different wall thicknesses at the workpiece. With a specific mandrel kinematic it is possible to produce tailored hollow shafts with varying cross-sections in their length direction as well as internal undercuts within one stroke of the ram. Similar approaches have been successfully tested in hot extrusion of aluminium [6, 7]. While the novel process offers significant advantages in terms of efficiency and geometric flexibility, the definition of the specific process parameters presents a major challenge. In particular, determining the necessary tool kinematic

This article is an open access article under the terms and conditions of the Creative Commons Attribution (CC BY) license (https://creativecommons.org/licenses/by/4.0)

to produce a specific target geometry is complex and currently relies on time-consuming iterative numerical simulations.

In recent years, Machine Learning (ML) approaches have been successfully applied in the field of metal forming to solve several similar complex problems [8, 9]. For example, neural networks were successfully employed to predict the initial billet geometry for a specific forged product [10] or to improve the modelling of friction in cold forging [11]. Furthermore, a neural network has been used for predicting the process energy in a multi-stage cold forging process [12]. Regarding tool kinematics, neural network approaches have been used to optimise and to predict a tool path strategy in dependence of the target geometry, blank dimensions and material type in incremental sheet metal forming [13, 14]. These examples demonstrate that ML approaches can be utilised for a deeper process understanding and, in particular, to predict tool kinematics.

Based on the potential of these data-driven strategies, this paper introduces a machine learning approach for predicting a tool kinematic for the novel cold forging process described above. The objective is to replace the time consuming iterative numerical procedure by the use of a neural network that is capable of directly predicting the mandrel kinematic for a specific target geometry of a tailored hollow shaft.

Material and Methods

In previous investigations, a numerical model in the FEM software DEFORM™-2D was developed and corresponding experiments have been conducted for its validation. Within the scope of these studies, flow curves of the test material AA 6082-O were also determined using the thermo-mechanical simulator Gleeble 3800c [5]. In the present investigation, the same material and numerical model were used. Figure 1a illustrates the setup of the numerical model, while Figure 1b depicts a schematic geometry of the pressed part, indicating the lengths L_1 to L_5. The variables L_1, L_3 and L_5 represent the axial lengths of the segments with a constant internal diameter and L_2 and L_4 are the axial lengths of the transitions between them.

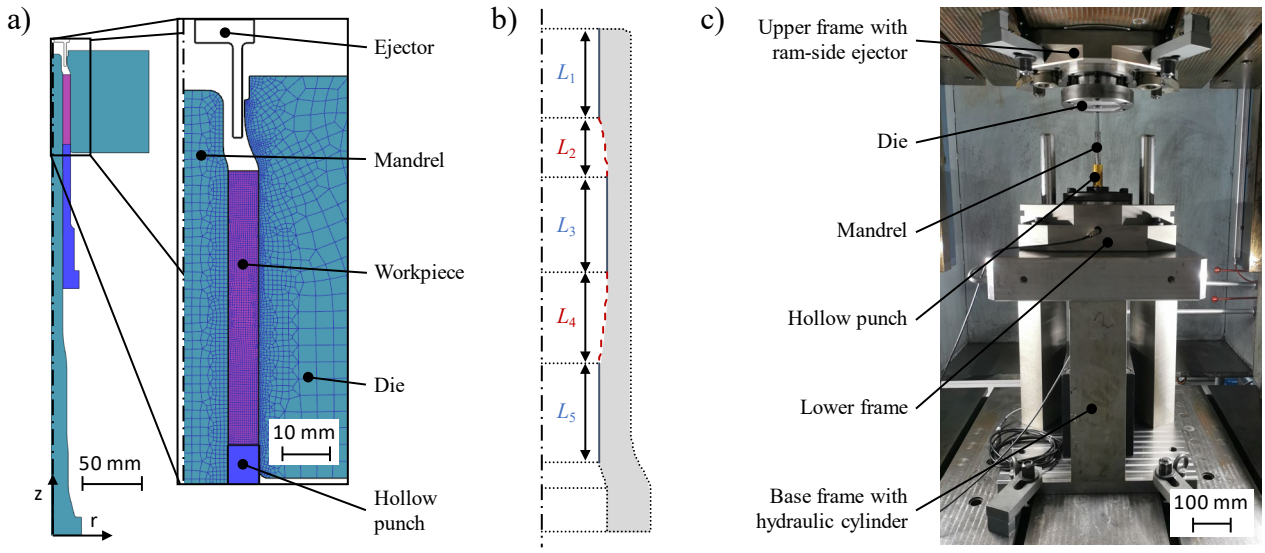

Fig. 1. a) Setup of the numerical model, b) schematic geometry of a pressed part, indicating the lengths L_1 to L_5 and c) tool setup for experimental investigation [5].

The workpiece was modelled as an elastic-plastic object having an outer diameter of 32 mm, an inner diameter of 19 mm and a length of 58 mm. The material properties were defined using the flow curves from [6], along with a Young's modulus of 70 GPa and a Poisson's ratio of 0.33 sourced from the same material in the DEFORM material library. The mandrel has a diameter of 19 mm which is reduced to 17 mm at its tip. The inner diameter of the die is 32 mm, reducing to 26 mm within the forming zone. The hollow punch is assumed as rigid and fixed, while the die is modelled as an elastic

body and moves with a constant velocity of -30 mm/s. This die velocity was chosen to enable the investigation of high relative velocities between the die and mandrel during the experiments. Shear friction model was used with $m = 0.15$ according to [5]. The workpiece mesh, comprising 2,000 elements with a minimum edge length of 0.1 mm, was determined through a convergence study and proven sufficient for the subsequent geometry analysis. Remeshing was performed whenever the interference depth between the workpiece and tool meshes exceeded half of the minimum element edge length, ensuring consistent mesh quality throughout the simulation. Mandrel and die were modelled with 1,500 and 1,300 elements, while considering mesh-windows for mesh refinement at the contact surfaces with the workpiece.

After simulating the forming process, a springback simulation was also conducted. In this step, the mandrel, die and ejector were removed and the final geometry including elastic springback effects was calculated. In contrast to the mandrel being rigid in [5], in this paper the mandrel is modelled as an elastic object. This approach offers a further improvement of the mandrel position control as well as the numerical representation of the axial position of the process-specific underfilling on the outer surface of the pressed part. For the die and mandrel, an elasticity modulus of 207 GPa and a Poisson's ratio of 0.3 were assumed based on common tool materials from the DEFORM material library.

For the experimental investigations the same tooling setup as described in [5] was used, as shown in Figure 1c. The experiments were conducted on a hydraulic press SMG HPZUI/300/300–1300/1000 with a maximum capacity of 6,000 kN. The tool setup comprises a base frame with a separate hydraulic cylinder for the movement of the mandrel, while the hollow punch is mounted on the fixed frame and the die is connected to the ram. The position of the hydraulic cylinder and respectively the mandrel is controlled as a function of the ram position. Zinc stearate was applied to the billets as a lubricant. To monitor the process, load cells and displacement sensors were used to acquire the forces and positions of the mandrel, hollow punch and die. For the experimental validation of the neural network, three different target geometries were selected. The geometrical analysis of the pressed parts was performed using a GOM ATOS Compact Scan 5M optical measurement system. The system provides a point spacing of 0.02 mm and was calibrated before the measurements. Furthermore, several repeated measurements were conducted for each pressed part.

During the forming process the mandrel moves independently from the die. Its path is defined by five support points P1 to P5. Each support point represents a mandrel position $s_{m,i}$ at a respective time t_i. The support points are linearly connected. Figure 2 illustrates the process sequence with the different mandrel positions for each support point P1 to P5 as well as the ejection stage with removed mandrel, die and ejector. The diagram shows the tool position versus process cycle time for the die and an exemplary mandrel kinematic profile (Kin_0001).

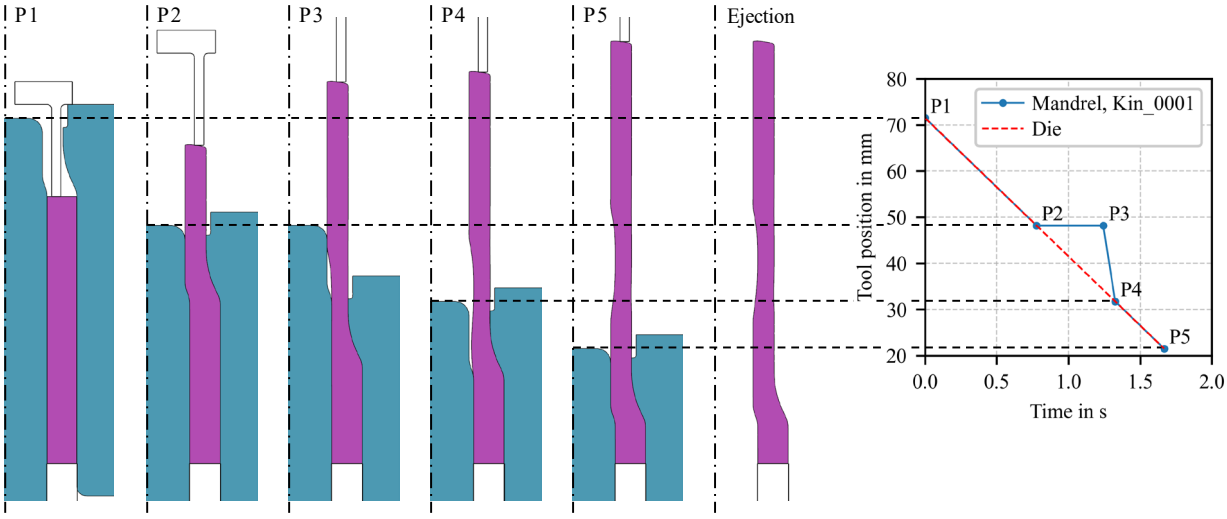

Fig. 2. Process sequence with the different mandrel positions for each support point P1 to P5 as well as the ejection with removed mandrel, die and ejector.

The mandrel movement starts and ends synchronised with the die, which is mounted directly to the ram. Consequently, the velocities $v_{m,12}$ (between P1 and P2) and $v_{m,45}$ (between P4 and P5) of the mandrel equal -30 mm/s. This results in the constraint that support points P1, P2, P4 and P5 must be located on the diagonal line connecting P1 and P5, which corresponds to the constant movement of the ram. The process initiation in the simulation refers to a ram position of $s_{r,1}$ = 1138.6 mm and t_1 = 0 s, while the process concludes after a stroke of 50 mm at $s_{r,5}$ = 1088.6 mm and t_5 = 1.6667 s. Figure 3a shows the mandrel kinematic in relation to time and Figure 3b shows the mandrel kinematic in relation to the ram position. Due to the geometric constraints of the tool setup and the synchronised movement of the ram and mandrel at the start and end of the process, the initial mandrel position was set to $s_{m,1}$ = 71.5 mm, resulting in a final position of $s_{m,5}$ = 21.5 mm.

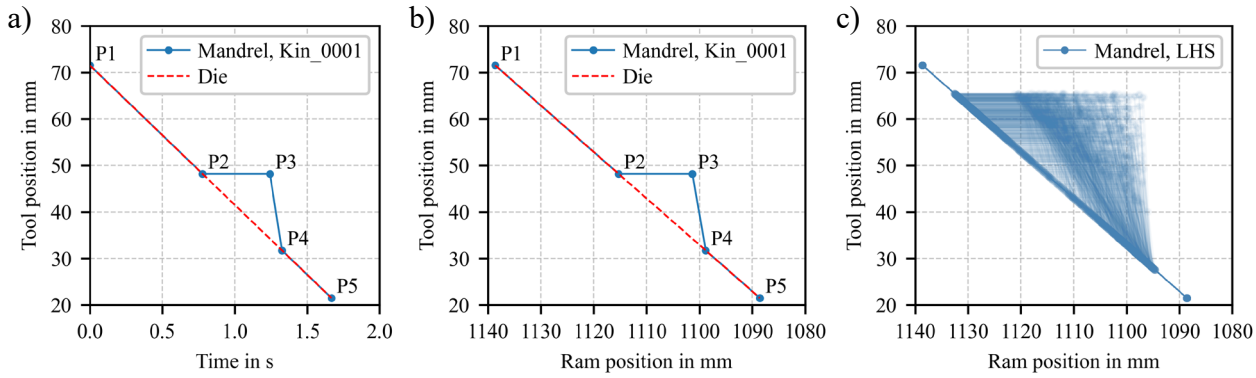

Fig. 3. a) Tool position vs. time for mandrel kinematic Kin_0001 and die, b) Tool vs. ram position for same mandrel kinematic Kin_0001 and die and c) generated Latin Hypercube Sampling (LHS).

To ensure a certain minimum length for the segments L_1 and L_5, the minimum time interval between P1 and P2 was defined to 0.19 s which leads to a minimum length of L_1 = 6.7 mm and between P4 and P5 to 0.18 s which leads to a minimum length of L_5 = 10.6 mm. These constraints were established based on initial numerical simulations to guarantee full contact between the workpiece and the mandrel. This ensures the formation of a section with a constant diameter of 17 mm and a sufficient length to clearly distinguish the cylindrical segment from the transition zones. Thus, the minimum value for t_2 is 0.19 s and the maximum value for t_4 is 1.4867 s. Between P2 and P3 the mandrel remains stationary and, therefore, the position $s_{m,2}$ is equal to $s_{m,3}$, while the minimum time interval between P2 and P3 was defined to 0.36 s. Similar to the sections with the smaller diameter of 17 mm, this minimum duration was selected to ensure the formation of a clearly defined cylindrical region with the larger diameter of 19 mm, allowing for a reliable geometric characterisation.

Taking these constraints into account, the entire kinematic profile of the mandrel can be defined by the three parameters t_2, t_3 and t_4. Conventionally, determining the specific combination of these parameters to achieve a desired target geometry requires an iterative numerical procedure. This involves simulating the process with a kinematic profile, analysing the resulting geometry, adjusting the parameters and re-simulating several times. Such a procedure is highly time-consuming and computationally expensive. However, as demonstrated in the state of the art, ML approaches can offer a robust solution for the prediction of tool kinematics in forming processes. Consequently, this study adopts such a data-driven approach to replace the iterative search for the geometry-specific tool kinematic. To generate a sufficient dataset of numerical results for the training of the neural network, 1,000 parameter combinations for t_2, t_3 and t_4 were created using Latin Hypercube Sampling (LHS), as shown in Figure 3c. This results in 1,000 distinct mandrel kinematics, labelled as Kin_0001 to Kin_1000. This sample size was selected to ensure a high sampling density within the multidimensional design space (three time values t_2 to t_4 and five respective lengths L_1 to L_5), providing a robust basis for the model to capture the relationships between the kinematics and the final geometry. For each kinematic, a simulation was carried out using the DoE tool of the FEM software DEFORM™-2D.

The resulting cross-section of the workpiece geometry, as defined by the radial and axial coordinates, was exported from each simulation run. Subsequently, contours within the radial coordinate ranges of $r = 8.5 \pm 0.02$ mm and $r = 9.5 \pm 0.02$ mm were identified with a Python code. This allowed for the direct determination of lengths L_1, L_3 and L_5 and the calculation of the transition lengths L_2 and L_4.

Since the simulation results could not be fully anticipated during the definition of the constraints for the input parameters, a post-simulation filtering step was necessary prior to the dataset preparation for the subsequent training of the neural network. This process discarded simulations that resulted in an output variable value of $L_3 = 0$ mm or a geometric overlap between segments L_2 and L_4. After this filtering step, finally 918 simulations remained for the initial dataset. This dataset was randomly divided into three subsets: a training dataset (70%), a validation dataset (15%) and a test dataset (15%). As the values of t_2 to t_4 are already within a narrow time frame (approximately 0.19 s to 1.48 s), a normalisation was considered unnecessary and the raw data with their physical units were used directly for training. To address this supervised regression task, the neural network uses the five input parameters L_1 to L_5 and the three output variables t_2, t_3 and t_4. It consists of three hidden layers with 32, 64 and 32 neurons using the ReLU activation function. The training was performed using the Adam optimiser to minimise the Mean Squared Error (MSE) loss function, with a batch size of 32 for a total amount of 1,000 epochs. The final hyperparameters and network structure were determined by an iterative refinement procedure.

Results and Discussion

Prediction of kinematic.

Figure 4 shows the parity plots for the output parameters t_2, t_3 and t_4 of the neural network designed for the prediction of the mandrel kinematic. In the plots, the predicted values from the neural network are compared to the true values. The results for the training, validation and test datasets are shown for each parameter.

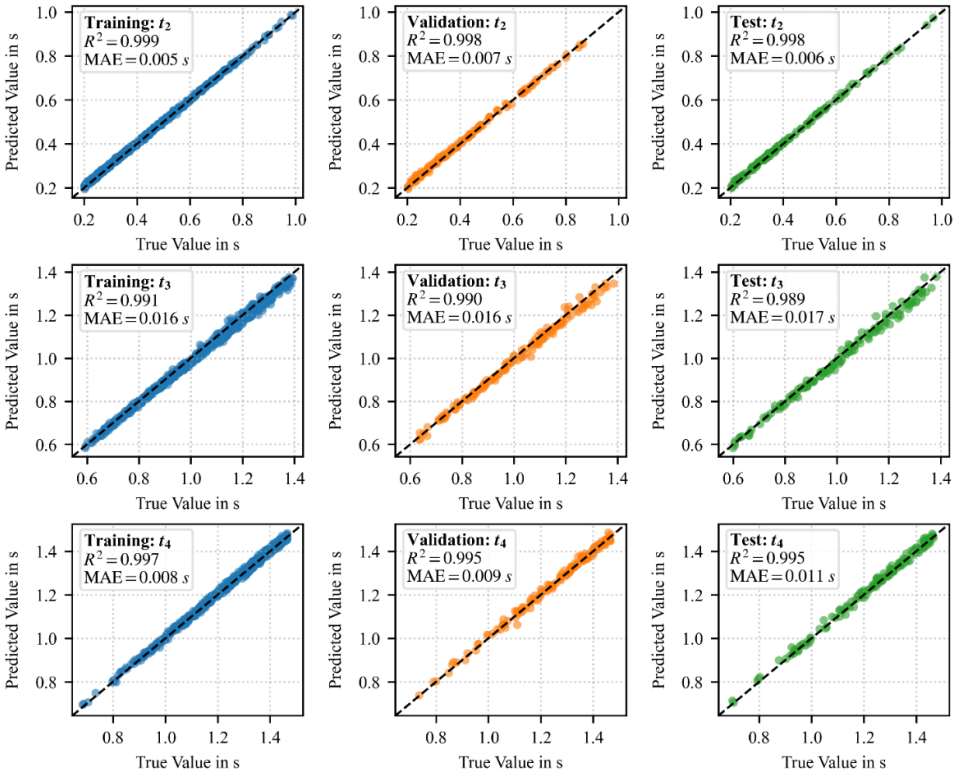

Fig. 4. Parity plots of the output parameters t_2, t_3 and t_4 of the neural network for the kinematic prediction.

Each diagram includes the respective coefficient of determination (R^2) and the mean absolute error (MAE) as performance metrics. The black dashed line represents the ideal identity line where the predicted and true values are identical. The slightly uneven distribution of points within the value range can be attributed to the specific constraints applied for the sample generation with LHS. Across all three parameters and datasets, the R^2 values range between 0.989 and 0.999. The maximum MAE observed for t_2, t_3 and t_4 are 0.007 s, 0.017 s and 0.011 s, respectively.

The learning curves depicted in Figure 5 show the MSE for training and validation dataset over 1,000 epochs. The logarithmic representation illustrates the convergence of the training and a high degree of generalisation of the model after the 1,000 epochs with a MSE of the training dataset of 6.447×10^{-5} s^2 and a slightly higher MSE of the validation dataset of 1.159×10^{-4} s^2. Furthermore, the unseen test dataset also provided high R^2 values. In conclusion, the predicted values are in good agreement with the true values, demonstrating that the trained model provides quite accurate predictions for the support points of the mandrel kinematic.

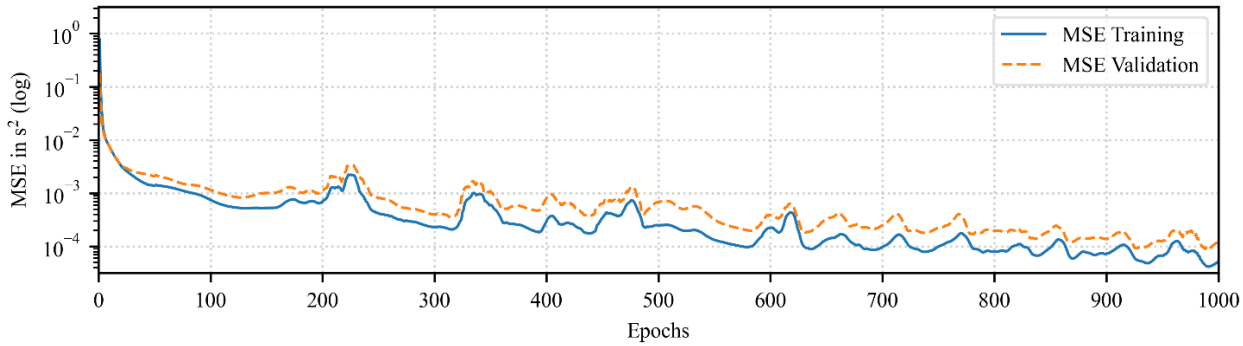

Fig. 5. Learning curve showing the MSE for training and validation dataset over 1,000 epochs.

A graphical user interface (GUI) has been developed to allow for the practical use of the trained neural network. This GUI enables the definition of the target geometry by entering values for the parameters L_1 to L_5. Figure 6 shows the GUI with the input of L_1 to L_5 in the upper left area, the prediction of the kinematic below and a simplified 2D and 3D representation of the target geometry to the right.

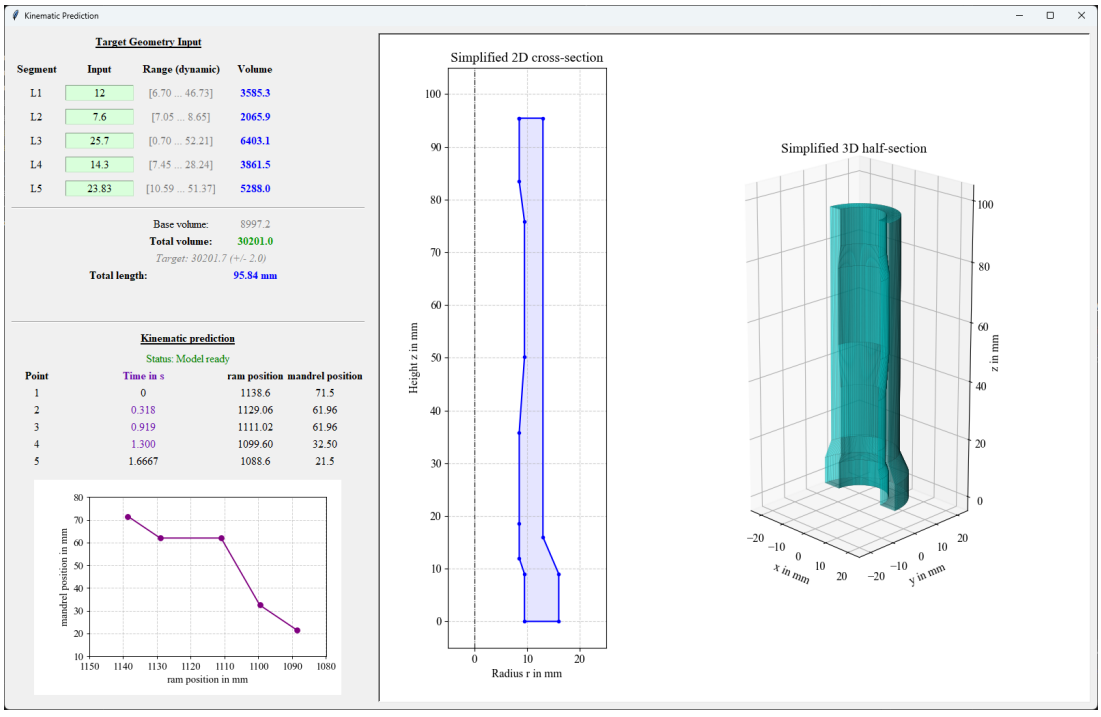

Fig. 6. Developed GUI with integrated trained neural network for prediction of the mandrel kinematic.

Based on the used training dataset each parameter is restricted to a specific value range enclosing a minimum and maximum value. The definition of these ranges is based on the physical feasibility constraints of the forming process, ensuring that the predicted geometries remain within manufacturable limits. Thus, only values within these ranges are accepted. Additionally, as the billet geometry dimensions are constant, the parameters L_1 to L_5 are constrained by the maximum available total volume. To take this into account, a real-time calculation is performed after each entry to determine the used volume for the segment of the respective L_i and the remaining volume for the other segments.

Consequently, the permissible input range for the remaining L_i adjusts dynamically with every input, while the minimum required volume for each segment is reserved initially. When any four of the five L_i parameters have been entered, the length of the final segment is automatically calculated and inserted based on the remaining volume. In this process, the lower section of the workpiece (starting from the lower end to the end of the shoulder) is always treated as a constant geometry with a fixed volume fraction. After entering the desired lengths, the neural network which is integrated into the GUI automatically outputs the time values for the mandrel kinematic.

Experimental Validation.

Following the training of the neural network and the development of the GUI, three target geometries were defined for the experimental validation. These geometries were selected in order to ensure that the lengths L_1, L_3 and L_5 exhibit distinct variations, thus representing a substantial part of the numerical design space that has previously been investigated. The input values L_1 to L_5 and output values t_2 to t_4 of the neural network for the three target geometries are depicted in Figure 7a. The corresponding calculated ram positions $s_{r,1}$ to $s_{r,5}$ and mandrel positions $s_{m,1}$ to $s_{m,5}$ of the support points P1 to P5 are depicted in Figure 7b.

a)

Input values in mm

Variable	Kinematic 1	Kinematic 2	Kinematic 3
L_1	12.00	34.30	9.30
L_2	7.60	7.70	7.50
L_3	25.70	11.70	9.10
L_4	14.30	11.37	16.50
L_5	23.83	15.40	38.22

Output values in s

Variable	Kinematic 1	Kinematic 2	Kinematic 3
t_2	0.318	0.742	0.254
t_3	0.919	1.221	0.691
t_4	1.300	1.412	1.055

b)

Ram and mandrel position of support points in mm

Variable	Kinematic 1	Kinematic 2	Kinematic 3
$s_{r,1}$	1138.60	1138.60	1138.60
$s_{r,2}$	1129.06	1116.35	1130.98
$s_{r,3}$	1111.02	1101.98	1117.86
$s_{r,4}$	1099.60	1096.23	1106.94
$s_{r,5}$	1088.60	1088.60	1088.60
$s_{m,1}$	71.50	71.50	71.50
$s_{m,2}$	61.96	49.25	63.88
$s_{m,3}$	61.96	49.25	63.88
$s_{m,4}$	32.50	29.13	39.84
$s_{m,5}$	21.50	21.50	21.50

Fig. 7. a) Input and output values of the neural network for the prediction of the mandrel kinematic and b) ram and mandrel position of the support points.

For each geometry the predicted kinematic was entered into the control system of the hydraulic cylinder to define the movement of the mandrel during the ram stroke and the parts were pressed. Subsequently, the pressed parts were cut into 270° segments to measure the inner and outer geometry using the GOM ATOS Compact Scan 5M optical measurement system. From the acquired 3D measurement data, 2D cross-sections were exported. The simplified 2D cross-sections from the kinematic prediction GUI with linear connection of the main points and photos of the cut 270° segment of the pressed parts for the kinematics 1 to 3 are shown in Figure 8a-c.

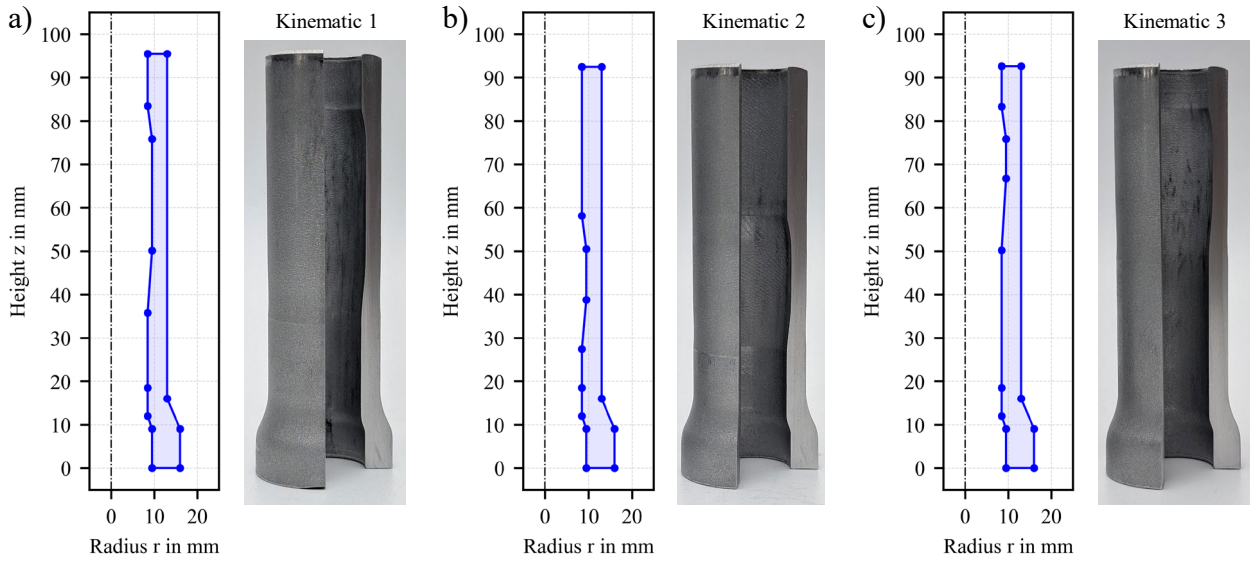

Fig. 8. Simplified 2D cross-section from GUI and cut 270° segment of the pressed part for a) kinematic 1, b) kinematic 2 and c) kinematic 3.

The segment lengths were then determined from the measured 2D cross-sections following the same procedure used for the analysis of the numerically obtained geometries. Table 1 presents the comparison between the target and measured values for L_1 to L_5 for the three test kinematics 1, 2 and 3. Additionally, the absolute errors (AE) for each L_i and mean absolute errors (MAE) are provided. An analysis of the deviations from the target values reveals a maximum AE of 0.60 mm for L_5 in kinematic 1, 0.67 mm for L_3 in kinematic 2 and 0.89 mm for L_5 in kinematic 3. Regarding the minimum deviations, the results show a minimum AE of 0.02 mm for L_3 in kinematic 1, 0.04 mm for L_4 in kinematic 2 and 0.21 mm for L_4 in kinematic 3. The MAE for kinematics 1 to 3 are 0.31 mm, 0.30 mm and 0.47 mm.

Table 1. Comparison of target and measured values of the variables L_1 to L_5 for three test kinematics, including absolute errors and mean absolute errors (in mm).

	Test kinematic 1			Test kinematic 2			Test kinematic 3		
Length	Target	Measured	AE	Target	Measured	AE	Target	Measured	AE
L_1	12.00	12.30	0.30	34.30	33.75	0.55	9.30	9.54	0.24
L_2	7.60	7.74	0.14	7.70	7.87	0.17	7.50	7.79	0.29
L_3	25.70	25.72	0.02	11.70	12.37	0.67	9.10	9.81	0.71
L_4	14.30	14.78	0.48	11.37	11.41	0.04	16.50	16.71	0.21
L_5	23.83	23.24	0.59	15.40	15.33	0.07	38.22	37.33	0.89
		MAE	0.31		MAE	0.30		MAE	0.47

The results show that by using the predicted kinematics, geometries with an MAE of the lengths L_1 to L_5 of less than 0.47 mm were obtained across the three tested variants. These observed deviations can be attributed to several factors. The numerical model was validated before with one specific kinematic. Afterwards the simulations with the LHS were conducted with the valid FEM model. Though, there are still uncertainties remaining such as friction variation due to, e.g., inhomogeneous lubrication or deviations of the idealised elastic properties of tools and workpiece and the real properties. In addition, the rather low ram velocity of -30 mm/s was necessary to ensure that the additional hydraulic cylinder could achieve its required relative velocity with respect to the ram. However, this velocity is at the lower end of the possible range for the used hydraulic press. For this reason, the velocity was not held constant and varied significantly throughout the entire process. Likewise, the pressure build-up of the hydraulic press was considerably delayed at such low ram velocities, which led to even more drops in velocity. In fact, the experimentally determined ram velocity varied in a range from -4 mm/s to -17 mm/s which can be seen in the velocity plot over the

ram position for the mandrel and the die in Figure 9a, although a value of -30 mm/s was set in the control unit of the hydraulic press. These rather low and inhomogeneous ram velocities resulted in a deviation of the numerically calculated and experimentally obtained strain rate within the process.

The predicted time values contain some inaccuracies as well. These inaccuracies are amplified when converting the predicted time values into the mandrel's control positions, as they are multiplied by the ram velocity (factor 30). Furthermore, the numerical model uses a piecewise linear kinematic profile with sharp transitions at the five support points. In reality, however, the hydraulic system executes these movements with smooth, continuous transitions. Finally, delays within the hydraulic control system led to deviations between the ideal and the actual experimentally obtained kinematic profile. Figure 9b shows the position of the die and the ideal and experimentally obtained positions of the mandrel on the left ordinate as well as the deviation between the two on the right ordinate. All values are depicted in relation to the ram position in accordance with Figure 3b. Direct comparison of Figure 9a with Figure 9b shows that the difference between the ideal and experimental mandrel positions is greatest in the transition regions during acceleration and deceleration. During these phases, deviations of up to 0.5 mm are observed.

Despite these deviations induced by the machine, the results demonstrate that the developed model can be used as an effective predictive tool. Based on a target geometry, the required kinematics can be determined immediately, eliminating the need for several initial trial-and-error simulations. However, machine-dependent adjustments are still necessary and, unfortunately, cannot always be compensated for. In the future, replacing the hydraulic system with a mechanical actuation system would enable a more precise control of the mandrel movement, thereby minimising machine-induced deviations.

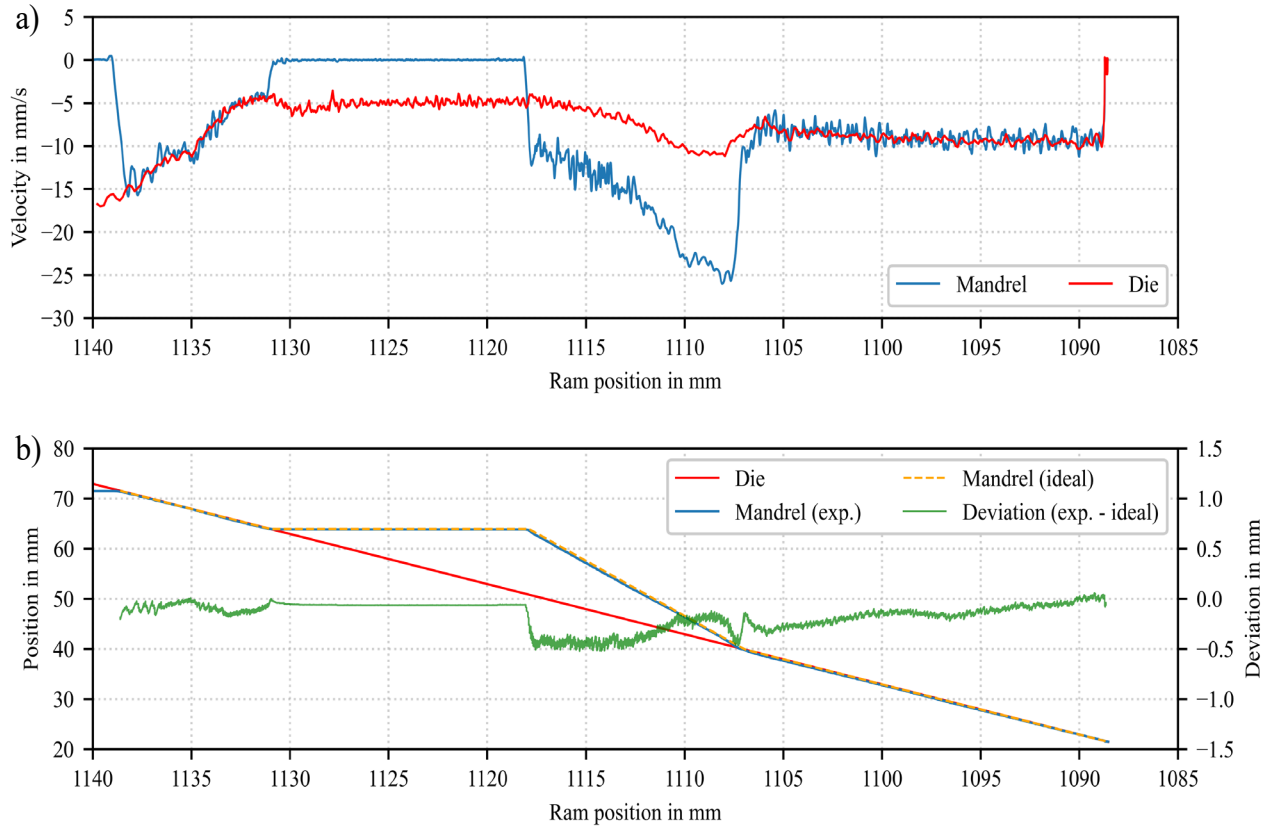

Fig. 9. a) Velocity of the mandrel and the die in relation to the ram position and b) positions of the die and the ideal and experimentally obtained positions of the mandrel as well as the deviation between the ideal and experimentally obtained positions of the mandrel position in relation to the ram position.

Conclusion and Outlook

In this contribution, an approach for a ML-based prediction of tool kinematics in cold forging of tailored hollow shafts with variable wall thickness is presented. Based on a numerical model of the cold forging process, a kinematic variation was conducted using the DoE tool in the FEM software DEFORM™-2D. A total of 1,000 kinematic variants were created with a LHS, taking specific process boundaries into account. The 2D cross-sections of the numerically calculated workpiece geometries were analysed to determine specific segment lengths of the workpiece. Using these geometric values alongside the corresponding time values which define the mandrel kinematic, a dataset for the training of a neural network was created. Instead of iteratively testing different mandrel kinematics to achieve a certain part geometry, this neural network enables the prediction of the required mandrel kinematic based on a specific target geometry. For the prediction of the three time values t_2, t_3 and t_4 for the mandrel kinematic, R^2 values between 0.989 and 0.999 were obtained with a maximum MAE ranging from 0.007 s to 0.017 s.

Subsequently, the trained model was integrated into a GUI which allows a user to enter a target geometry of a part and provides the predictions for the mandrel kinematic. For three selected target geometries the respective mandrel kinematics were predicted and used in an experimental setup to validate the prediction. The pressed parts were optically measured and the results were compared to the predicted geometry. For the three target geometries a MAE of all characteristic lengths ranging from 0.30 mm to 0.47 mm was observed. Consequently, the developed model significantly reduces the need for several trial-and-error simulations. However, potential for optimisation remains, particularly regarding machine-induced deviations.

Future works could focus on reducing the remaining inaccuracies to optimise the prediction quality. Thus, replacing the hydraulic system with a mechanical actuation system is suggested to enable a more precise control of the mandrel movement, thereby minimising machine-induced deviations. Finally, the model could be extended to cover a wider range of geometric variants. Although the current model is limited to the specific 'thick-thin-thick' wall thickness profile, the methodology presented in this paper can be adapted to other geometric profiles.

Acknowledgment

The research project “Development of a cold forging process for manufacturing hollow parts with variable wall thicknesses” (fund number ZF4012808LP9) in cooperation with the company LS-Mechanik GmbH was funded by the Federal Ministry of Economic Affairs and Energy through the German Federation of Industrial Research Associations (AiF) as part of the Central Innovation Programme for SMEs (ZIM) based on a decision of the German Bundestag. The authors would like to thank the German Federation of Industrial Research Associations for the financial support and the project partner LS-Mechanik GmbH for the collaboration.

References

[1] D. M. Sassoli and J. P. Matos Fernandes, Regulation (EU) 2021/1119 of the European Parliament and of the Council of 30 June 2021 establishing the framework for achieving climate neutrality and amending Regulations (EC) No 401/2009 and (EU) 2018/1999 ('European Climate Law'), Official Journal of the European Union (2021).

[2] H.-P. Degischer and S. Lüftl (Eds.), Leichtbau: Prinzipien, Werkstoffauswahl und Fertigungsvarianten, Erste Auflage, Wiley-VCH Verlag, Weinheim, 2012. ISBN: 9783527659869.

[3] Hans-Willi Raedt (Ed.), Massivumgeformte Komponenten, Zweite Auflage, Hirschvogel Holding GmbH, 2014.

[4] A. Weiss, M. Arny and M. Liewald, Impact of a Splined Mandrel Geometry on Die Filling in a Cold Forging Process with Adjustable Deformation Zone, KEM 926 (2022) 612–620. DOI: 10.4028/p-aynwq8.

[5] A. Weiß and M. Liewald, Cold Forging of Hollow Shafts with Variable Wall Thickness by Means of an Adjustable Forming Zone, Numerical Methods in Industrial Forming Processes, Lecture Notes in Mechanical Engineering, ISBN: 978-3-031-58005-5, Springer International Publishing (2024) 185–194. DOI: 10.1007/978-3-031-58006-2_14.

[6] M. Negendank, S. Müller and W. Reimers, Extrusion of Aluminum Tubes with Axially Graded Wall Thickness and Mechanical Characterization, Procedia CIRP 18 (2014) 3–8. DOI: 10.1016/j.procir.2014.06.098.

[7] T. Makiyama and M. Murata, Controlling Inside Diameter of Circular Tube by Extrusion, MSF 396-402 (2002) 513–520. DOI: 10.4028/www.scientific.net/MSF.396-402.513.

[8] M. Liewald, T. Bergs, P. Groche, B.-A. Behrens, D. Briesenick, M. Müller, P. Niemietz, C. Kubik and F. Müller, Perspectives on data-driven models and its potentials in metal forming and blanking technologies, Prod. Eng. Res. Devel. 16 (2022) 607–625. DOI: 10.1007/s11740-022-01115-0.

[9] J. Cao, M. Bambach, M. Merklein, M. Mozaffar and T. Xue, Artificial intelligence in metal forming, CIRP Annals 73 (2024) 561–587. DOI: 10.1016/j.cirp.2024.04.102.

[10] D. Kim, B. Kim and J. Choi, Determination of the initial billet geometry for a forged product using neural networks, Journal of Materials Processing Technology 72 (1997) 86–93. DOI: 10.1016/S0924-0136(97)00134-9.

[11] S. Volz, J. Launhardt and P. Groche, Advanced friction modelling for cold forging using a feed forward neural network, Tribology International 211 (2025) 110837. DOI: 10.1016/j.triboint.2025.110837.

[12] P. Tchasse and M. Liewald, Monitoring and prediction of the process energy in multi-stage cold forging using recurrent and self-attention based neural networks, Int J Adv Manuf Technol 142 (2026) 431–441. DOI: 10.1007/s00170-025-17052-y.

[13] A. Fiorentino, G.C. Feriti, E. Ceretti, C. Giardini, C. Bort and P. Bosetti, Development of Tool Path Correction Algorithm in Incremental Sheet Forming, KEM 622-623 (2014) 382–389. DOI: 10.4028/www.scientific.net/KEM.622-623.382.

[14] D. Opritescu and W. Volk, Automated driving for individualized sheet metal part production—A neural network approach, Robotics and Computer-Integrated Manufacturing 35 (2015) 144–150. DOI: 10.1016/j.rcim.2015.03.006.

The publication of this article was funded by the University of Stuttgart